Available online at www.sciencedirect.com
ScienceDirect
Journal of Power Sources 166 (2007) 112–119
JOURNAL OF POWER SOURCES
www.elsevier.com/locate/jpowsour

Application of infrared thermal imaging to the study of pellet solid oxide fuel cells

D.J.L. Brett [a], P. Aguiar [b], R. Clague [c], A.J. Marquis [c], S. Schöttl [d], R. Simpson [d], N.P. Brandon [b,*]

[a] *Department of Chemical Engineering, Imperial College London, UK*
[b] *Department of Earth Science and Engineering, Imperial College London, UK*
[c] *Department of Mechanical Engineering, Imperial College London, UK*
[d] *Engineering and Process Control Division, National Physical Laboratory, Teddington, UK*

Received 17 July 2006; received in revised form 11 December 2006; accepted 28 December 2006
Available online 17 January 2007

Abstract

The application of infrared thermal imaging to the study of solid oxide fuel cells is demonstrated. The temperature increase accompanying polarisation of gadolinium doped ceria pellet cells is measured and the effect of temperature increase on polarisation characteristics is modelled. Temperature increases of the order of 2.5 °C were measured for heavily loaded pellet cells. Measurement accuracy of 0.1 °C and spatial resolution of 0.5 mm allow temperature distribution heterogeneity to be clearly discerned. A total heat transfer coefficient is derived from experimental results that allow the development of a model that predicts the extent of self-heating. For pellet fuel cells, self-heating is not expected to have a large effect on the polarisation characteristics; however, for thin electrolytes and high current density the effect becomes appreciable.

Keywords: Pellet fuel cell; Solid oxide fuel cell; Temperature mapping; Thermal imaging

1. Introduction

Solid oxide fuel cells (SOFCs) are high temperature fuel cell variants that employ oxide ion conducting ceramic electrolytes operating in the temperature range of 500–1000 °C [1]. These devices show excellent potential for a broad range of power generation applications and particularly for large scale and residential combined heat and power (CHP). However, elevated temperature operation imparts certain challenges with regard to factors such as ensuring sealing integrity and minimising mechanical stresses due to thermal expansion coefficient mismatch. Cells and stacks may suffer from significant temperature variation during operation that will lead to performance limitation. The ability to accurately measure the temperature distribution of SOFC systems and components is thus a powerful research and design tool for the advancement of this technology.

As a non-contact method, infrared (IR) thermal imaging does not disturb the behaviour of the fuel cell, it allows measurements on operational fuel cells, provides high spatial resolution (<1 mm) that generates detailed data sets suitable for model input and has fast acquisition time that enables dynamic phenomena to be studied.

This paper reports work performed to assess areas in which infrared thermometry can be applied to SOFCs, and discusses how the resulting thermal images can be used to develop models that predict the effect of temperature on electrochemical performance. Application of the technique to the thermo-mechanical analysis of SOFCs will be the subject of a future publication.

1.1. Thermal imaging of fuel cells

Incorporation of temperature measuring devices (e.g. thermocouples and thermistors) is necessary for proper control, test and operation of fuel cells. This ranges from the crude placement of a single sensor to highly instrumented arrangements that allow 2D mapping of a single cell or plate-by-plate profiling of stacks [2].

* Corresponding author. Tel.: +44 20 7594 5704; fax: +44 20 7594 7444.
E-mail address: n.brandon@imperial.ac.uk (N.P. Brandon).

0378-7753/$ – see front matter © 2007 Elsevier B.V. All rights reserved.
doi:10.1016/j.jpowsour.2006.12.098

In order to get an accurate measure of the temperature of a cell and detect temperature changes as they happen at the electrode, it is necessary to place the sensor as close to the electrodes (or electrolyte) as possible. However, incorporation of thermocouples close to the interface of current collector and electrode may lead to membrane penetration in a polymer electrolyte fuel cell (PEFC) or cracking of an SOFC during cell assembly or heat-up. For PEFCs, thin film temperature sensors have been developed that allow *in situ* measurement within the membrane electrolyte [3]; however, this is not practical for SOFCs.

Adzic et al. [4] have used a 'flat type' thermocouple to probe the temperature distribution at the cathode of a planar SOFC. The thermocouple was placed in close proximity (as close as 5 μm), but not in contact with the electrode surface and a spatial resolution of 0.5 mm was achieved. Localised hot spots were measured that were as much as 16 °C above the mean surface temperature.

An alternative to discreet temperature sensors is the use of infrared measurements. This technique has the advantage of not requiring sensor placement or connecting leads, and high spatial resolution and frame collection rates can be achieved. The technique is ideal for measuring the outer surface temperature of a fuel cell or stack; however, in order to investigate the temperature within a fuel cell, the construction needs to be modified to allow optical access to the surface of interest (i.e. electrode surfaces).

Infrared thermal imaging has been performed on PEFCs using IR transparent windows made from zinc selenide (>75% transmission over 8–12 μm) [5] and barium fluoride (>85% transmission over 8–12 μm, although a correction was still performed) [6]. These studies showed that significant temperature variation results across the surface of a PEFC due to variation in current density, humidification and reactant composition. The work of Wang et al. [6] demonstrates how electrode surface temperature increases with current density. For a current density of 1.38 A cm^{-2} a maximum spatial distribution of ca. 6 °C was observed over the 2.9 cm × 3.9 cm electrode surface, with over 10 °C temperature rise recorded in some parts of the electrode. These results show that it is important to have a measure of the temperature at the electrode of the fuel cell since the bulk fuel cell temperature and electrode temperature can vary significantly (over 8 °C in this study). In addition, it was also reported that a significant time was necessary for the electrode to reach a stable temperature after a current step change. Over 1800s was required in this instance in order for the heat generated to radiate through the test cell to the environment [6].

1.2. Pellet fuel cells

For materials development and investigation of different fuels, so-called 'pellet' or 'button' SOFCs are routinely employed; see Ref. [7] for an example of their use. These are normally electrolyte supported devices (typ. 250–1500 μm in thickness) with screen-printed or painted anode and cathode and metallic gauze current collectors. The active surface area is typically of the order of 1 cm^2. A reference electrode is sometimes incorporated in order to explicitly determine the performance of the anode and cathode [8].

Pellet cells are not intended for technological applications, but rather for screening purposes. The relatively thick electrolyte support and ambient-air 'breathing' cathode usually precludes high performance. However, their small size and homogeneous reactant supply to the electrodes allows the useful assumption that current density and temperature are spatially invariant. It is also generally assumed when analysing pellet cell results that the temperature does not change when the cell is polarised. This is important since even a small change in temperature can lead to an appreciable change in electrolyte conductivity or electrochemical activity. In this work, the temperature distribution characteristics of operating pellet cells are examined and the assumptions about their behaviour considered.

Pellet fuel cells operating in the 'intermediate' temperature (IT) range of 500–650 °C are considered in this study [9]. This temperature regime of operation has the advantage of allowing more rapid start-up and shut-down; reduced rates of corrosion; simplified system requirements and lower component cost compared with high temperature SOFCs. To achieve the requisite performance at lower temperatures, materials are required that have superior conductivity and electrochemical activity than conventionally employed SOFC materials. In this case, gadolinium doped ceria (CGO) is used as the electrolyte [10], Ni/CGO cermet as the anode, and $La_{1-x}Sr_xCo_yFe_{1-y}O_{3-\delta}$ (LSCF), a perovskite based on $LaCoO_3$ and specially developed for IT-SOFC operation, as the cathode [8].

2. Experimental

2.1. Materials preparation

Cylindrical electrolyte pellets were produced by uniaxially pressing $Ce_{0.9}Gd_{0.1}O_{1.95}$ powder (Rhodia) at 1 tonne (30 s), followed by sintering at 1450 °C in air for 2 h. Pellets with a thickness of 0.35 mm and a diameter of 16 mm were prepared.

The anode cermet slurry was prepared using a 40 wt.% $Ce_{0.9}Gd_{0.1}O_{1.95}$ (CGO-10) and 60 eq.wt.% of Ni in the form of green NiO (Alpha Aesar) mixed with various additives including binders, dispersant, plasticizer and solvent. The doctor blade technique was used to coat the electrode onto the electrolyte which, after being sintered and reduced at 1300 °C in air for 2 h, had a thickness of 60 μm. Each pellet was initially reduced in 10% H_2/N_2 (+2.3% H_2O) as the electrodes were raised from ambient to working (550–650 °C) temperature.

The cathode was $(La_{0.6}Sr_{0.4}Co_{0.2}Fe_{0.8}O_{3-\delta})$/30 wt.% CGO10 paint coated to give a final thickness of ca. 30 μm. The area specific resistance (ASR) of the cathode was calculated from symmetrical cell ac impedance measurements to be 0.84 Ω cm^2 at 600 °C. Current collectors were affixed to the electrodes using some additional electrode material and sintering. Pt gauze was used as the current collector on the anode side and Au gauze on the cathode, both 0.06 mm wire diameter and 0.25 mm aperture. Pt must be used at the anode due to the requirement of a higher sintering temperature.

Both the anode and the cathode were deposited with a diameter of 1 cm, giving a geometric surface area of 0.785 cm^2.

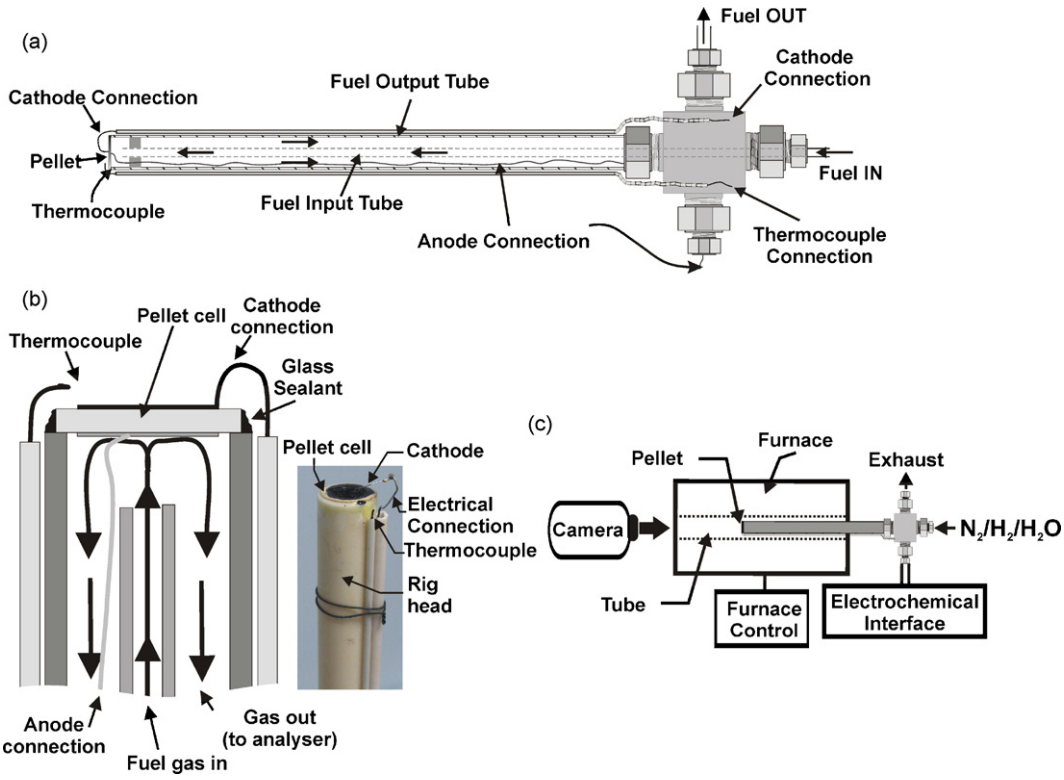

Fig. 1. Pellet cell testing setup. (a) Pellet cell rig showing inner fuel supply tube; (b) pellet cell attachment to the rig tube; (c) positioning of IR camera and test rig inside of furnace.

2.2. Fuel cell pellet testing

Fuel cell pellet testing was performed using the setup shown in Fig. 1. This system allows N_2 and H_2 (both 'zero grade', BOC) to be introduced to the anode of the fuel cell, humidification of the gas took place by bubbling through a column of water to give a vapour content of 3.2%. Thermal mass flow controllers (Bronkhorst, UK) were used to deliver the reactants to the fuel cell. The fuel cell pellets were bonded to the end of the test rig alumina tube using glass sealant (Dielectric IP 041, Heraeus, UK) painted onto the non-coated outer ring on the anode side of the pellet. Sprung tie-rods were used to hold the pellet and rod together. A K-type thermocouple was positioned next to the pellet to monitor ambient temperature. Electrochemical measurements were performed using a Solartron 1286 electrochemical interface running CorrWare (Solartron Analytical, UK). Gold wire with a diameter of 0.5 mm was used to make the electrical connection between the electrodes and the outside of the furnace, after which coaxial cable is used to connect to the potentiostat with voltage sense connections to correct for voltage drop in the current carrying cables. With a total of 30 cm within the furnace, the potential drop in the gold wire was calculated to be ~20 mV at the maximum current density measured.

2.3. Infrared temperature measurement

The imaging data were obtained using a Cedip Silver infrared camera. This camera is based on an InSb focal plane array detector. The detector is cooled to below 80 K by an internal Stirling cooler. It is sensitive to infrared radiation with wavelengths from 3 to 5 μm. For temperatures above 200 °C a narrow band filter was used, which limited the sensitivity to the range of 3.97–4.01 μm. The image consists of 320 × 256 pixels and can be recorded at up to 100 Hz. In some cases up to 10 successive images were averaged to reduce the noise.

The camera was factory calibrated for a variety of different combinations of integration time, filters and lenses. This calibration includes corrections for non-uniformity of the detector array and bad pixel replacement. In this study, the factory calibration was used and the camera settings chosen accordingly.

The camera was used with a 27 mm lens and mounted on a bench-mounted translation stage. The sample distance was approximately 0.3 m from the camera, resulting in a spatial resolution of the order of 0.5 mm.

All experiments were monitored with a thermocouple located as close as possible to the sample. This also served as a cross-check for the thermal camera calibration. The thermocouple's cold junction was either placed in ice water or controlled at room temperature. The thermocouple had been annealed at 950 °C but not individually calibrated. Nevertheless consistent readings between the furnace control thermocouples, infrared camera and monitor thermocouple were obtained.

2.4. Furnace temperature control

Pellet fuel cell experiments were carried out in a horizontal tube furnace of 0.6 m length and an inner diameter of 40 mm. The furnace was temperature controlled using a thermocouple located between the sample space and the heaters. One end of

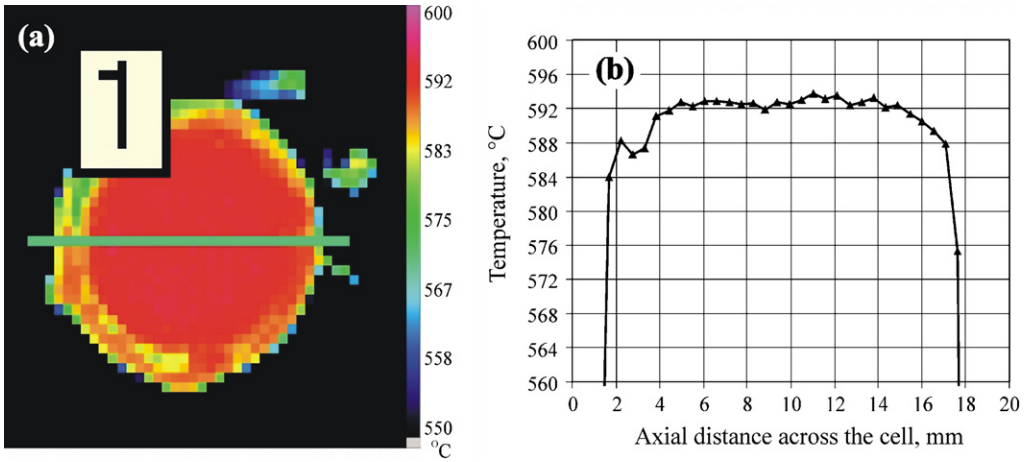

Fig. 2. Pellet SOFC at constant temperature: (a) thermal image in false colours; (b) temperature profile across the cell, along the line labelled '1' in the left panel. (For interpretation of the references to colour in text, the reader is referred to the web version of the article.)

the sample space was blocked using thermal wool and the other end was left open to allow optical access.

The thermal stability of the furnace was characterised with the monitor thermocouple. The furnace was tuned to achieve a 1 °C peak-to-peak oscillation. It is interesting to note that the furnace exhibits oscillations at a constant frequency of ca. 5 mHz. If electrochemical impedance measurements were made on the fuel cell down to this frequency, this would result in an artefact in the response. For this reason, it is prudent to characterise the temporal temperature variation of furnaces when electrochemical impedance measurements are being made.

Further information on the experimental details and other applications of IR thermometry to the study of SOFCs is available in [11].

3. Results

3.1. Pellet cell testing

3.1.1. Assessment of the measurement capabilities

Before proceeding with the presentation of the experimental results, it is valuable to assess the quality of the results obtained from the thermal imaging camera. For that purpose, before electrically loading the pellet cell, a thermal image was recorded at stable temperature. The image is shown in false colours in Fig. 2(a); red and magenta representing higher temperatures, blue representing lower temperatures. The central red area is the active (electrode) area of the SOFC.

For pellet cell testing, an emissivity of 1 was used for the cathode due to close agreement between IR and thermocouple values. The large number of cavities in the surface of the cathode due to the highly porous nature of the material is assumed to be the reason for the high emissivity.

A contrasting ring is observed around the electrode area that displays a lower temperature, this is the plain electrolyte material which has a lower emissivity and therefore radiates less infrared light and appears colder than it actually is. The thermocouple and current collecting wire are seen as artefacts around the central pellet image.

The temperature profile along the line drawn on the cell (labelled "1") is shown in Fig. 2(b). Apparent temperature variations within a range of 1 °C occur over the active area and are visible in the graph. They are found not to vary with time. Since there is no reason for a real temperature gradient over such

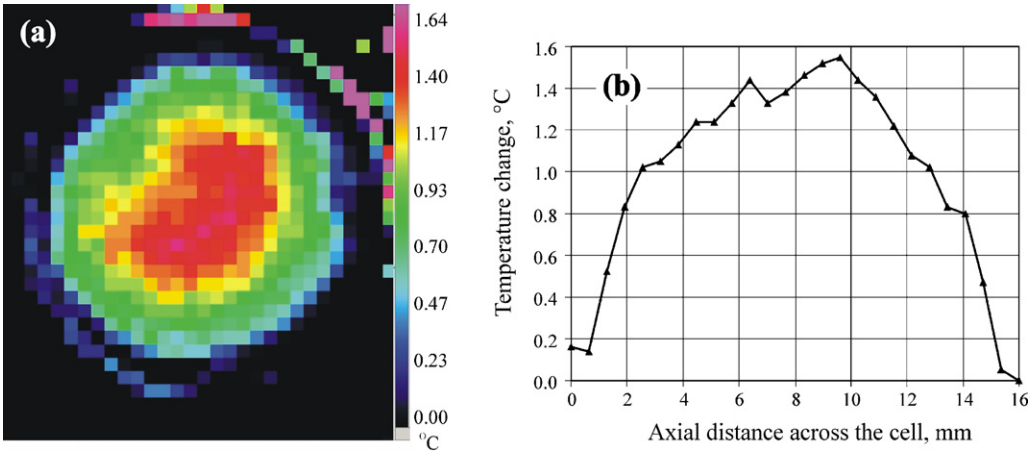

Fig. 3. Temperature change during a polarisation curve measurement at 592 °C: (a) temperature difference between open circuit and 0.2 V; (b) profile of this temperature difference across the cell.

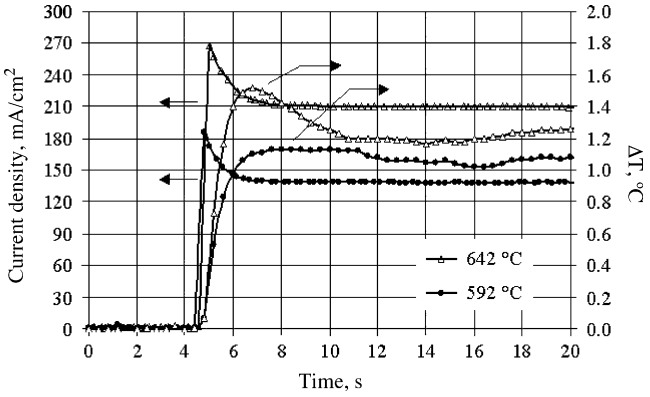

Fig. 4. Current density and temperature transients for a load change from OCV to 0.3 V.

small length scales, they are assumed to be a manifestation of the non-uniformity of the sample emissivity.

Fig. 3 presents the distribution of the temperature difference between the cell at OCV and at 0.2 V (nominal furnace temperature of 592 °C). A temperature increase of ca. 1.7 °C is observed in the centre of the cell, and most of the active area exhibits at least 1.0 °C temperature rise. The steepest gradient, approximately 0.7 °C mm^{-1}, appears around the edge of the active zone (electrode area). However, the temperature increase is not entirely symmetric; such temperature increase inhomogeneity may be the consequence, for example, of uneven current density, poor current collector contact, electrode delamination, or electrode/electrolyte thickness/composition variation.

Despite the small temperature changes (<2 °C) recorded at high ambient temperature values (ca. 600 °C), this measurement demonstrates a temperature resolution of less than 0.1 °C. The result also shows that non-uniformities in pellet cell temperature can occur and be detected on length scales of less than 1 mm.

All of the ensuing temperature difference values are the average values of 49 pixels in the centre of the pellet.

3.1.2. Fuel cell polarisation and self-heating

The relationship between fuel cell loading and temperature was investigated by performing voltage step changes and monitoring the current and temperature transients. Fig. 4 gives an example of the transients observed when the cell is stepped from OCV to 0.3 V for nominal operation at 592 and 642 °C.

Taking the steady state current and temperature and correcting it for the temperature oscillation of the furnace, the temperature increase and polarisation curve can be constructed as shown in Fig. 5. Before discussing the features of the polarisation curves and the temperature increase, and in order to appreciate the analysis in Section 4.1, it is useful to consider the efficiency losses exhibited by fuel cells.

As is well known, the open circuit voltage is the maximum voltage that can be achieved by a fuel cell under specific operating conditions. However, the voltage of an operating cell is lower than this. As current is drawn from a fuel cell, the cell voltage falls due to internal resistances and overpotential losses. These losses are common to all types of fuel cells and cannot be eliminated, although temperature, pressure, gas flow rate and

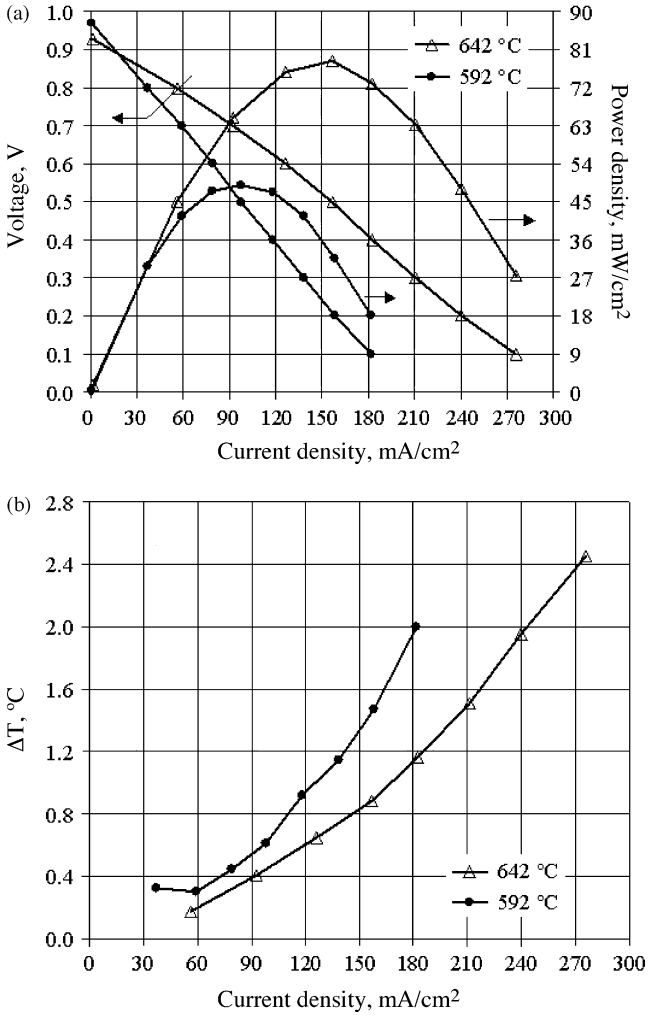

Fig. 5. (a) Polarisation curves for pellet cell at 592 and 642 °C and (b) temperature increase with current density.

composition, electrode and electrolyte materials, and cell design, all influence their magnitude. The voltage of an operating cell is generically given by Eq. (1), which can be derived from Kirchoff's and Ohm's laws by considering a fuel cell as many small elements in series, with each element acting as a power source with its own internal resistance.

$$U = U^{\mathrm{OCV}} - (\eta_{\mathrm{Ohm}} + \eta_{\mathrm{conc,electrodes}} + \eta_{\mathrm{act,electrodes}}). \quad (1)$$

η_{Ohm} represents the Ohmic losses and $\eta_{\mathrm{conc,electrodes}}$ and $\eta_{\mathrm{act,electrodes}}$ the anode and cathode concentration and activation overpotential losses, respectively.

Ohmic losses are caused by resistance to conduction of ions (through the electrolyte and electrodes) and electrons (through the electrodes and current collectors) and by contact resistance between cell components. This voltage drop is important in all types of cells and is essentially linear and proportional to current density.

Concentration overpotentials appear when mass transport effects hinder the electrode reaction, i.e. when the reactant inlet flux and the product outlet flux from an electrode are slower than that corresponding to the current drawn, and significant concen-

tration profiles develop across the electrodes. Physical processes that contribute to the occurrence of concentration overpotentials include gas species molecular transport in the electrode pores, solution of reactants into the electrolyte, dissolution of products out of the electrolyte, and diffusion of the reactants/products through the electrolyte to/from the reaction sites.

Activation overpotentials reflect the kinetics of reactions taking place at the anode and cathode. At high operating temperatures, the electrode reaction is rapid and, as a result, the activation overpotential is usually small. However, as the operating temperature falls, activation overpotentials can become the most significant cause of voltage drop.

As mentioned previously, the pellet cells analysed here use cerium gadolinium oxide (CGO) instead of the more common yttria stabilized zirconia (YSZ) as the electrolyte material. CGO has a higher ionic conductivity than YSZ at lower temperature, allowing practical fuel cell operation down to 500 °C. However, it is less chemically stable than YSZ and can undergo reduction at high temperatures and the fuel conditions typically experienced in an SOFC. Reduction leads to the CGO exhibiting some mixed ionic/electronic conductivity, resulting in an internal electronic short-circuit in the cell, loss of open circuit voltage, and a possible decrease in cell efficiency. The magnitude of the electronic leakage current through the electrolyte depends on a number of factors, such as: operating temperature, oxygen partial pressure gradient across the electrolyte, thickness of the electrolyte, ionic conductivity of the CGO, electrode polarisation resistance, and current density. The effect of current density is particularly pertinent, since as this increases the average oxygen partial pressure in the electrolyte also increases, reducing the electronic conductivity of the electrolyte and thus the electronic leakage current density. Therefore, it is generally found that, at practical operating current densities and at operating temperatures below around 600 °C, the electronic leakage current is negligible, and the efficiency of the cell not impaired [12].

As can be seen from Fig. 4, both the current density and the temperature overshoot when the voltage is stepped from OCV to 0.3 V, before stabilising at their steady state values. The current overshoot is due to an initial excess of reactant present at the anode before the development of a concentration gradient (where the hydrogen concentration is lower at the boundary than at the bulk) that results in a steady-state current. The temperature responds rapidly to the potential step change, overshoots and reaches equilibrium within 5 s of the initial perturbation. Since the thermal overshoot lags that of the current overshoot, the former is assumed to be a consequence of the latter.

Fig. 5(a) shows the polarisation curves at 642 and 592 °C for operation on moist hydrogen fuel (97% H_2, 3% H_2O). It can be seen that, although the general fuel cell performance decreases with decreasing temperature, the OCV increases from 0.929 to 0.970 V as the temperature decreases. This is consistent with the fact that the Nernst equation predicts an increase in OCV with decreasing temperature and that the electronic leakage current density is also predicted to decrease, thus contributing to a further increase in the OCV. At 592 °C a maximum power output of 48.9 mW cm^{-2} was measured while at 642 °C a maximum power of 78.3 mW cm^{-2} was observed.

Fig. 5(b) shows the temperature difference between the temperature of the sample cell and the temperature of the furnace corresponding to the polarisation curves in Fig. 5(a). It can be seen that, in accordance with that described above, ΔT increases as more current is drawn out of the cell, given that voltage losses increase and thus the excess heat generated also increases. Also, it is seen that for lower operating temperatures (furnace temperatures) the ΔT is higher. This corroborates the fact that fuel cells are less efficient at lower temperatures thus delivering lower current densities but generating more excess heat.

It should be remembered that IR thermometry measures the surface temperature of the sample. This technique does not provide information on temperature distribution through the thickness of the pellet cell. However, given that the electrolyte thickness is significantly larger than the cathode, it is reasonable to assume that the cathode/electrolyte interface and electrolyte temperature is close to that measured using the camera. It is believed that for a sample with this geometry, the temperature variation through the thickness of the cell will not be as extreme as that observed laterally across the electrode. However, future work will explicitly consider the anode side of the cell and extend the analysis to consider temperature change accompanying rapid redox cycling of the electrode.

4. Discussion

4.1. Effect of temperature increase on polarisation characteristics

Distortion in the polarisation characteristics of pellet fuel cells has been accounted for by the self-heating effect of reaction and current flow [8]. Here, experimental observations and a fuel cell model are used to determine the effect of cell heating on polarisation plots.

The various sources of voltage loss that can occur in a fuel cell have been described in Section 3.1.2. Temperature generally plays an important role in determining the magnitude of these losses, which normally decrease with increasing temperature. As is well-known, in addition to electric power, heat is also produced in a fuel cell. The local heat produced (W m^{-2}) can be given by

$$\text{Local heat produced per area} = (-\Delta H)_{\text{elect}} R_{\text{elect}} - P_{\text{SOFC}} = (-\Delta H)_{\text{elect}} \frac{j}{2F} - jU. \quad (2)$$

where P_{SOFC} (W m^{-2}) is the local power density, $(\Delta H)_{\text{elect}}$ (J mol^{-1}) is the enthalpy change of the reaction taking place and R_{elect} (mol m^{-2} s^{-1}) is the reaction rate. Eq. (2) is simply the difference between the enthalpy released by the exothermic electrochemical reactions and the local power density withdrawn from the cell, and can also be expressed by:

$$\text{Local heat produced per area} = \frac{j}{2F} T(-\Delta S)_{\text{elect}} + j(\eta_{\text{Ohm}} + \eta_{\text{conc,electrodes}} + \eta_{\text{act,electrodes}}) \quad (3)$$

where $(\Delta S)_{elect}$ ($J\,mol^{-1}\,K^{-1}$) stands for the entropy change. Thus, the excess local heat produced in a fuel cell is due to the entropy change of the electrochemical reactions and to all the potential losses mentioned above.

4.1.1. Model of temperature increase with polarisation

One of the questions that this investigation aims to answer is whether the temperature increase due to self-heating of pellet fuel cells can be predicted, and by how much this temperature increase affects the interpretation of polarisation results. To investigate this, a simplified model that aids in the prediction of the temperature increase when measuring the polarisation curves was developed; this model was then used to assess the effect of changes in temperature on polarisation curves simulated using representative electrode and electrolyte properties. Eq. (4) shows the heat balance for the sample pellet cell under the experimental set up described in Section 2.2. This assumes that all the reported values in Fig. 4 are at steady-state and accounts for heat transfer both by convection (between the pellet cell and both the fuel and air flow) and radiation (between the pellet cell and furnace walls), as well as for the excess heat generated in the cell. Thermal conduction between the electrolyte pellet and the ceramic tube holder (via the glass sealant) was not considered since even for the worse case scenario in which the edge of the electrolyte pellet increased in temperature by the same amount as the centre of the electrode (for which there is no evidence from the thermal imaging results), heat dissipation via this mechanism would account for less than 1% of the total.

$$h_{total}(T_{pellet} - T_{furnace}) + \sigma\varepsilon(T_{pellet}^4 - T_{furnace}^4) - \left[(-\Delta H)_{elect}\frac{j}{2F} - jU\right] = 0 \quad (4)$$

$h_{total} = h_{fuel} + h_{air}$ ($J\,m^{-2}\,s^{-1}\,K^{-1}$) represents the global heat transfer coefficient for both the air and the fuel side, T_{pellet} and $T_{furnace}$ (K) the pellet and furnace temperatures, respectively, σ the Stefan–Boltzmann constant ($W\,m^{-2}\,K^{-4}$), and ε the pellet emissivity. It was assumed that the fuel impinging onto the anode and the air at the cathode were all at the temperature of the furnace. Given that the experimental data provides values for the pellet and furnace temperatures and for the voltage and current density, Eq. (4) was used to calculate the total heat transfer coefficient for each set of experimental points. The heat transfer coefficient values obtained were $1179\,J\,m^{-2}\,s^{-1}\,K^{-1}$ (± 30) and $1017\,J\,m^{-2}\,s^{-1}\,K^{-1}$ (± 55) for 642 and 592 °C, respectively.

In order to predict the effect of temperature increase with current density on the polarisation characteristics of the pellet fuel cell, a previously reported model [12] was modified to incorporate Eq. (4). In this model a total heat transfer coefficient of $1100\,J\,m^{-2}\,s^{-1}\,K^{-1}$ has been used. The model takes into account all the voltage losses described above, i.e. Ohmic resistance, concentration overpotentials, activation overpotentials and electronic leakage current. The cylindrical pellet cell geometry and corresponding dimensions used in the experiment were applied to the model, while all other parameters used in Ref. [12] have remained constant to embody representative values for a practical IT-SOFC.

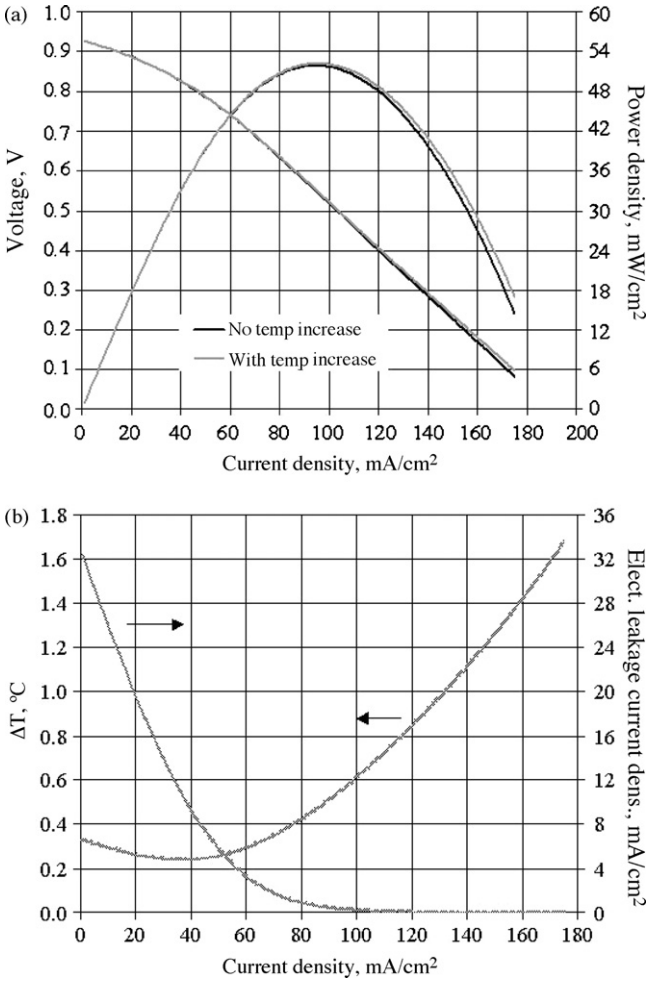

Fig. 6. Predicted (a) polarisation curves and (b) temperature difference (between the temperature of the cell and the temperature of the furnace) and electronic leakage current density for a 350 μm pellet cell at 600 °C.

Fig. 6(a) shows the polarisation curve predicted by the model at 600 °C, with and without the increase in temperature considered, for an electrolyte thickness of 350 μm. It can be seen that temperature increase has a minor effect on the polarisation response compared to the isothermal case. Fig. 6(b) shows the temperature increase and electronic leakage current density change with ionic current density. It can be seen that the temperature increase is minor and that the electronic current is negligible under normal operating conditions (typ. 0.6–0.8 V) but increases under open circuit and low current conditions.

The same cell parameters were applied to a cell with a thin electrolyte (30 μm) to assess the effect of current on cell self-heating. The results obtained are presented in Fig. 7 where a maximum temperature increase of around 12 °C is seen to have an appreciable effect on the polarisation characteristics. For such a system, determination of cell performance parameters (i.e. electrode kinetics) would require consideration of the fuel cell temperature change in order to derive accurate values. This result also shows that self-heating and electronic leakage phenomena can significantly change the polarisation response compared to the generally assumed constant temperature case.

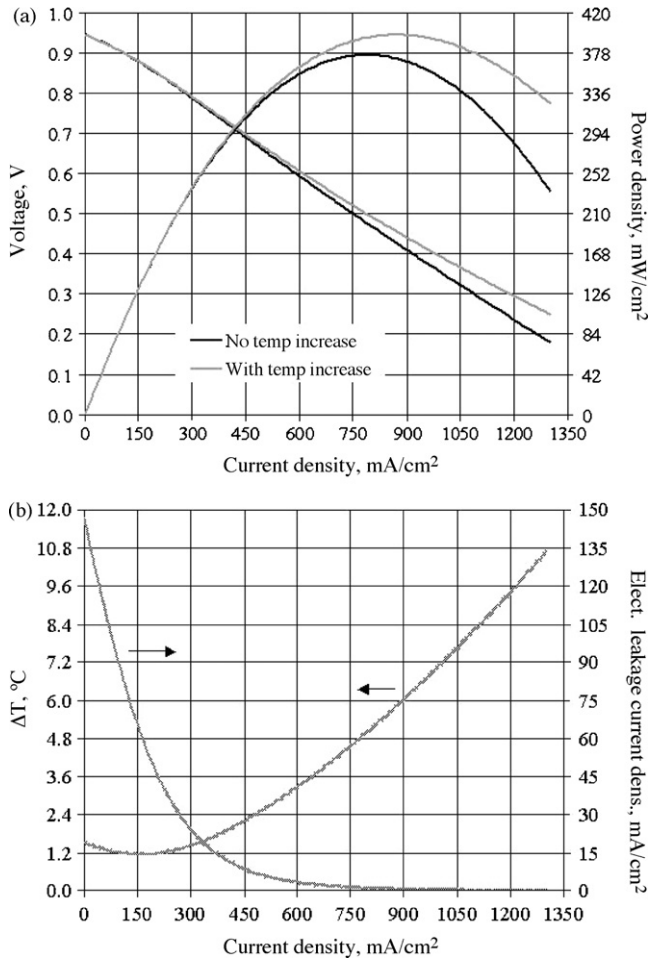

Fig. 7. Predicted (a) polarisation curves and (b) temperature difference (between the temperature of the cell and the temperature of the furnace) and electronic leakage current density for a 30 μm pellet cell at 600 °C.

5. Conclusions

Infra-red thermometry has been applied to the study of operational IT-SOFCs to determine the temperature changes and spatial distribution associated with different current densities for electrolyte supported pellet cells.

Temperature changes of up to 2.5 °C were observed for heavily loaded pellet cells. Evidence of temperature distribution heterogeneity was observed at low cell voltage, although this was not significant for cells operating over typical polarisation limits. The effect of cell heating on polarisation characteristics was investigated using a model, and the total heat transfer coefficient derived from experimentation. For a CGO electrolyte supported pellet cell with a thickness of 350 μm, the cell heating effect on the polarisation response is not significant. Thinner electrolytes, suitable for technologically relevant SOFCs, show an appreciable temperature increase that is beneficial to electrochemical performance but not suitable for the accurate measurement of electrode performance. Collectively, the electrochemical and temperature measurements made suggest that electrolyte-supported pellet cells provide a reasonable means of assessing cell performance and that the assumptions made about their operation are valid for most circumstances.

Acknowledgments

The authors would like to acknowledge Denis Cumming for preparation of pellet cell electrolytes and Michael de Podesta, Gareth Hinds and Bob Rudkin for technical input.

This project was funded by the DTI under the Measurement for Emerging Technologies programme and the EPSRC SUPERGEN Fuel Cells programme.

References

[1] S.C. Singhal, K. Kendall, High-temperature Solid Oxide Fuel Cells: Fundamentals, Design and Applications, 1st ed., Elsevier, Oxford, 2003.
[2] D. Kim, J. Lee, T.-H. Lim, I.-H. Oh, H.Y. Ha, J. Power Sources 155 (2006) 203–212.
[3] S. He, M.M. Mench, S. Tadigadapa, Sens. Actuators A 125 (2006) 170–177.
[4] M. Adzic, M.V. Heitor, D. Santos, J. Appl. Electrochem. 27 (1997) 1355–1361.
[5] A. Hakenjos, H. Muenter, U. Wittstadt, C. Hebling, J. Power Sources 131 (2004) 213–216.
[6] M. Wang, H. Guo, C. Ma, J. Power Sources, in press.
[7] D.J.L. Brett, A. Atkinson, D. Cumming, E. Ramírez-Cabrera, R. Rudkin, N.P. Brandon, Chem. Eng. Sci. 60 (2005) 5649–5662.
[8] A. Esquirol, N.P. Brandon, J.A. Kilner, M. Mogensen, J. Electrochem. Soc. 151 (2004) A1847–A1855.
[9] B.C.H. Steele, Solid State Ionics 134 (2000) 3–20.
[10] B.C.H. Steele, Solid State Ionics 129 (2000) 95–110.
[11] S. Schöttl, D.J.L. Brett, Applications of Thermal Imaging to Solid Oxide Fuel Cell Research, NPL Report, DEPC-TH 007, 2006, ISSN 1744-0289.
[12] R.T. Leah, N.P. Brandon, P. Aguiar, J. Power Sources 145 (2005) 336–352.